Au_{13} Superatom Bearing Two Terpyridines at Coaxial Positions: Photoluminescence Quenching via Complexation with 3d Metal Ions

Naoki Kito,[1] Shinjiro Takano,[1] Shinya Masuda,[1] Koji Harano,[2] and Tatsuya Tsukuda*[1]

[1]Department of Chemistry, Graduate School of Science, The University of Tokyo,7-3-1 Hongo, Bunkyo-ku, Tokyo 113-0033, Japan
[2]Center for Basic Research on Materials, National Institute for Materials Science (NIMS), 1-1 Namiki, Tsukuba 305-0044, Japan
E-mail: <tsukuda@chem.s.u-tokyo.ac.jp>

Naoki Kito
Naoki Kito received his M.S. degree in 2023 from The University of Tokyo under the supervision of Prof. Tatsuya Tsukuda. His research interest is the atomically precise synthesis and functionalization of ligand-protected gold clusters.

Tatsuya Tsukuda
Tatsuya Tsukuda received his Ph.D. degree in 1994 from The University of Tokyo under the supervision of Prof. Tamotsu Kondow. After postdoctoral research at RIKEN, he was appointed Assistant Professor at The University of Tokyo in 1994 and he became an Associate Professor at the Institute for Molecular Science in 2000. In 2007, he was promoted to Professor at the Catalysis Research Center of Hokkaido University, and in 2011 he moved to The University of Tokyo. His research interests cover the atomically precise synthesis and characterization of stabilized gold clusters and their catalytic applications.

Abstract

A gold cluster $[Au_{13}(dppe)_5(EPTpy)_2]^{3+}$ (dppe = 1,2-bis(diphenylphosphino)ethane, EPTpy-H = 4'-(4-ethynylphenyl)-2,2':6',2"-terpyridine) was synthesized by ligand exchange reaction of $[Au_{13}(dppe)_5Cl_2]^{3+}$. Single-crystal X-ray diffraction analysis revealed that two terpyridyl moieties were σ-bonded to the coaxial positions of the icosahedral Au_{13} core. These two terpyridyl moieties were coordinated with 3d metal ions M^{2+} (M = Co, Ni, Cu, Zn) in acetonitrile solution under ambient conditions. The photoluminescence (PL) of $[Au_{13}(dppe)_5(EPTpy)_2]^{3+}$ with a quantum yield of 0.17 at ~780 nm was almost completely quenched by coordination with Co^{2+}, Ni^{2+}, and Cu^{2+}, while the PL was not affected by Zn^{2+} coordination. The metal-dependent PL quenching behavior is ascribed to the difference in the electronic structure of the metal ions. The energy transfer from the Au_{13} chromophore to the coordinated Co^{2+}, Ni^{2+}, or Cu^{2+} with an open electronic structure proceeds efficiently via an electron exchange mechanism, while the process is prohibited for Zn^{2+} with a closed electronic structure.

Keywords: Au_{13} superatom, terpyridines, photoluminescence

1. Introduction

Monolayer-protected gold clusters (AuMPCs) are promising building units for functional materials[1-4] because of their unique physicochemical properties that can be tuned by various structural parameters including size and atomic packing of the Au core, doping to the Au core, and nature of the surface ligands.[1–7] The next challenge in this research field is to design and construct well-defined systems composed of AuMPCs by a bottom-up approach to produce collective functions for various applications. There are reports on the fabrication of one-, two-, and three-dimensional assemblies of AuMPCs using a variety of intercluster interactions[8-11] such as hydrogen bonding of the ligands,[12] aurophilic interaction[13,14] and multidentate ligation to the Au cores.[15,16] However, we have not yet found reports on the self-assembly of AuMPCs via chelation of metal ions.

The aim of this work was to design and synthesize AuMPCs bearing terpyridyl moieties that can efficiently chelate various metal ions in a tridentate manner.[17,18] By controlling the number and location of the terpyridyl moieties on the Au core, it is possible to construct AuMPCs-based systems with well-defined structures in a programmable manner. For example, if two terpyridyl moieties are introduced at the coaxial position of AuMPCs, the AuMPCs can be self-assembled into linear polymers, similarly to metallo-supramolecular polymers.[19–21] AuMPCs can incorporate a given number of metal ions by complexation to the terpyridyl groups. The electronic interaction between AuMPCs and coordinating metal ions via the conjugated system will modify the optical properties of the constituent chromophores of the Au core and terpyridyl–ion moieties. Conversion and transport of the photon energy acquired at the chromophore are also expected within the coordination complex of AuMPCs and metal ions.

To prove the above concept, we attempted to introduce a terpyridine-functionalized alkynyl ligand (4'-(4-ethynylphenyl)-2,2':6',2"-terpyridine, EPTpy-H; Scheme 1a) to a diphosphine-protected Au_{13} cluster $[Au_{13}(dppe)_5Cl_2]^{3+}$ (**1**, dppe = 1,2-bis(diphenylphosphino)ethane) via a ligand exchange approach.[22] Cluster **1** is an ideal platform because two Cl ligands replaceable with alkynyl are located at the coaxial position (Scheme 1b) and efficient photoluminescence (PL) is exhibited at ~800 nm with a quantum yield (QY) of ~0.11.[22–24] Electrospray ionization mass spectrometry (ESI-MS) revealed

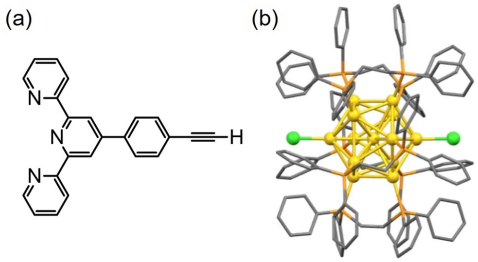

Scheme 1. (a) Chemical structure of EPTpy-H. (b) Crystal structure of **1**.[23] H atoms are omitted, and carbon and phosphorus atoms of dppe moieties are shown as sticks for clarity. Color code: yellow, Au; orange, P; gray, C; green, Cl.

the formation of $[Au_{13}(dppe)_5(EPTpy)_2]^{3+}$ (**2**) by mixing **1** and an excess amount of EPTpy-H under basic condition. Single-crystal X-ray diffraction (SCXRD) analysis of **2** showed that two EPTpy ligands were successfully introduced at the coaxial positions of the icosahedral Au_{13} core. The PL QY of **2** was enhanced to ~0.17. The reaction of **2** with two molar equivalents of 3d metal ions M^{2+} (M = Co, Ni, Cu, Zn) led to the complexation of two M^{2+} ions to **2**, as revealed by ESI-MS and X-ray absorption spectroscopy (XAS). The PL of **2** was almost completely quenched by specific complexation with Co^{2+}, Ni^{2+}, and Cu^{2+} ions having an open 3d electron configuration. The energy transfer mechanism from the photoexcited Au_{13} core to the coordinated M^{2+} ion was proposed to explain the PL quenching.

2. Experimental

2.1. Materials

4'-(4-Bromophenyl)-2,2':6',2"-terpyridine, dppe, 2,2':6',2"-terpyridine (tpy), and trimethylsilylacetylene were purchased from Tokyo Chemical Industry. Tetrahydrofuran and nickel(II) nitrate hexahydrate were purchased from Kanto Chemical Company. Acetonitrile was purchased from Merck KGaA. Palladium(II) acetate was purchased from Sigma Aldrich. $(AuCl)_2(dppe)$,[25] $[Au_{13}(dppe)_5Cl_2](PF_6)_3$,[23] EPTpy-H,[26] and $[Co(tpy)_2](PF_6)_2$[27] were synthesized according to the literature procedures. Other chemicals were purchased from FUJIFILM Wako Pure Chemical Industries. The water used was Milli-Q grade (>18 MΩ). All commercially available reagents were used without further purification.

2.2. Synthesis

EPTpy-H (167.6 mg), acetonitrile (50 mL), and acetone (10 mL) were mixed in a test tube and stirred at 55℃ for ~10 min. After EPTpy-H was fully dissolved, **1**·$(PF_6)_3$ (50.8 mg) and triethylamine (69.7 μL) were added. The reaction mixture was stirred at 55°C for 24 h. The crude mixture was cooled to room temperature, and an ethanolic solution of $NaPF_6$ (16.7 mg in 10 mL) was added to the mixture. After stirring was stopped, the reaction mixture was evaporated to dryness. The solid was washed with methanol and toluene. Then, it was dissolved in acetone (15 mL) and poured into toluene (150 mL) through a syringe filter. The precipitates were collected by suction filtration and washed with toluene and diethyl ether. **2**·$(PF_6)_3$ (33.2 mg, 58%) was obtained as a dark red solid. The crystal suitable for SCXRD analysis was grown by vapor diffusion of diethyl ether to the solution of **2** in acetonitrile/methanol = 1/2.

2.3. Characterization

Positive-mode ESI mass spectra were recorded on a Bruker compact ESI-Q-TOF mass spectrometer. The mass spectra were calibrated with $[Cs(CsI)_n]^+$ clusters as external references, generated from a 99% aqueous methanol solution of CsI (0.5 mg/mL). All the mass spectra were recorded using an acetonitrile solution. The isotope patterns were calculated by mMass software.[28] Ultraviolet-Visible (UV-Vis) absorption spectra were recorded with a JASCO V-630 spectrophotometer in the transmission mode using a quartz cell with an optical path length of 1 cm. PL spectra were recorded by a JASCO PL-6600 fluorophotometer using a capped quartz cell with an optical path length of 1 cm. All the PL spectra were recorded at the excitation wavelength of 525 nm and normalized by the absorbance at 525 nm. PL lifetime measurements were conducted using a picosecond fluorescence lifetime measurement system (Hamamatsu Photonics). A 371 nm laser diode with a pulse width of 103 ps was used for the excitation and a C4780 streak camera with a monochromator was used for the 2D detection of PL signals. The obtained PL decay profiles were fitted with a single exponential function. All the optical measurements were conducted in an acetonitrile solution under air at room temperature unless otherwise noted. $^{31}P\{^1H\}$ (162 MHz) nuclear magnetic resonance (NMR) spectra were recorded with a JEOL JNM-ECS400 spectrometer at 298 K. Chemical shifts in the $^{31}P\{^1H\}$ NMR charts were referenced to those of 85% H_3PO_4 (δ0.00) as an external standard. SCXRD experiments were performed on a Rigaku VariMax Dual diffractometer with a Pilatus 200K hybrid pixel array detector using CuKα radiation. The structure was refined using the full-matrix least-squares method on F^2 by SHELXL-2018[29] and disordered electron density was treated by SQUEEZE on the PLATON platform.[30,31] The CheckCIF program generated A- and B-level alerts regarding the residual electron densities near gold atoms. This is probably due to the insufficient absorption correction of thin crystals having a high absorption coefficient. Nevertheless, the structural features are not at all affected by these alerts. The structural information is summarized in Table S1 and the structure is deposited at the Cambridge Crystallographic Data Center (CCDC) with the deposition No. 2267045.

Co K-edge XAS measurements were carried out at room temperature in the transmission mode for $Co(NO_3)_2{\cdot}6H_2O$ and $[Co(tpy)_2](PF_6)_2$ or in the fluorescence mode for Co^{2+} complex of **2** using the BL01B1 beamline at the SPring-8 facility of the Japan Synchrotron Radiation Research Institute (Approval No. 2021A1200). The acetonitrile solution of the sample in a plastic cell was used for the fluorescence measurement. The X-ray energy was calibrated using Co foil.

Transmission electron microscopy (TEM) was conducted to see the multimers of **2** connected via Co^{2+} ions. Boron nitride nanotubes (BNNTs) purchased from BNNT Materials and purified according to the reported procedure[32] were used as supports since our preliminary measurement could not identify the 1D linked structure due to the poor dispersibility of **2** on the amorphous carbon film conventionally used for TEM. The TEM specimen was prepared as follows. First, acetonitrile solutions of **2** (0.025 mM; 10 mL) and $Co(NO_3)_2{\cdot}6H_2O$ (1.0 mM; 250 μL) were mixed at room temperature (**2**: Co^{2+} = 1:1). The mixed solution (1 mL) was transferred to a vial containing 0.1 mg of purified BNNT. Then, the dispersion was heated at 80℃ for 1 h and sonicated in a bath sonicator for ~5 min. Finally, the solution was dropcast onto a carbon grid (RO-C15, Ohken Shoji), washed with acetonitrile, and dried in vacuum (4 hPa) for 30 min. The specimen was further heated at ~100℃ by an incandescent lamp for 10 min to remove amorphous contaminants. TEM observation was carried out on an aberration-corrected TEM instrument (FEI Titan Cubed) at an acceleration voltage of 40 kV under 4×10^{-6} Pa in the specimen column using a monochromator for an incident electron beam (ΔE = 0.15 eV). Images were captured and processed on a CMOS camera (Gatan OneView, in situ mode, 4096×4096 pixels) operating on a binning 2 mode. The images were recorded at under-focus conditions (defocus value: 6–10 nm). A series of images was continuously recorded at a frame rate of 25 frames per second at an electron dose rate of about 1×10^6 e^- nm^{-2} s^{-1},[34] and 50 consecutive images in the video were superimposed after drift correction to obtain a higher signal-to-noise-ratio image, which was then filtered using a bandpass filter (filtering structures smaller than 3 pixels and larger than 40 pixels, tolerance of direction: 5%).

2.4. Complexation Reaction

A given amount of metal salts ($Co(NO_3)_2{\cdot}6H_2O$, $Ni(NO_3)_2{\cdot}6H_2O$, $Cu(NO_3)_2{\cdot}3H_2O$, or $Zn(NO_3)_2{\cdot}6H_2O$) was added to the acetonitrile solution of **2**·$(PF_6)_3$. The progression of the complexation reaction was monitored by ESI-MS and spectroscopic measurements.

3. Results and Discussion

3.1. Synthesis and Characterization of $[Au_{13}(dppe)_5(EPTpy)_2]^{3+}$

A terpyridine-modified Au_{13} cluster $[Au_{13}(dppe)_5(EPTpy)_2]^{3+}$ (**2**) was synthesized by the ligand exchange reaction of **1** according to the literature procedure[22] with modification. An excess amount of EPTpy-H and triethylamine (Et_3N) was added to the acetonitrile–acetone solution of **1**. The stoichiometry of the reaction can be written as follows:

$$[Au_{13}(dppe)_5Cl_2]^{3+}\ (\mathbf{1}) + 2\ \text{EPTpy-H} + 2\ Et_3N \rightarrow [Au_{13}(dppe)_5(EPTpy)_2]^{3+}\ (\mathbf{2}) + 2\ Et_3N{\cdot}HCl \quad (1)$$

We used Et_3N as the base to deprotonate EPTpy-H instead of sodium methoxide[22] because Et_3N is easier to handle and the reaction can be done in acetonitrile–acetone solvent in which the decomposition of the Au_{13} clusters was suppressed. The prominent peak in the positive-mode ESI mass spectrum (Figure 1a) was assigned to $[Au_{13}(dppe)_5(EPTpy)_2]^{3+}$, which indicates the successful isolation of **2**. The $^{31}P\{^1H\}$ NMR spectrum of **2** (Figure S1) shows a single peak from the P atoms on dppe at 67.5 ppm. This observation indicates that all ten P atoms are equivalent in the NMR time scale. Vapor diffusion of diethyl ether to an acetonitrile–methanol solution of $\mathbf{2}{\cdot}(PF_6)_3$ afforded the single crystals. The geometric structure and chemical identity of **2** were determined by SCXRD analysis (Figure 1b, Table S1). Two EPTpy ligands were σ-bonded to the diagonal apex sites of an icosahedral Au_{13} core while the structure of the Au_{13} core and five dppe ligands on the surface was maintained during reaction (1). One of the EPTpy ligands (EPTpy(I) in Figure 1c) was nearly planar, while the other (EPTpy(II) in Figure 1c) was slightly distorted due to the packing with the dppe moieties of the adjacent **2** and PF_6^- in the single crystal (Figure S2). Notably, two EPTpy ligands take a nearly coplanar configuration, suggesting electronic coupling between two π systems of the EPTpy ligands and the superatomic orbitals of the Au_{13} core. A previous theoretical study on the related cluster $[Au_{13}(dppe)_5(PA)_2]^{3+}$ (PA-H = phenylacetylene) reported that the highest occupied molecular orbital (HOMO) is made of the C(2p) π orbital of the PA ligands and the 1P superatomic orbital of the Au_{13} core.[22] The terpyridyl moieties protrude from the protecting layers of dppe, allowing the complexation of metal ions without steric hinderance.

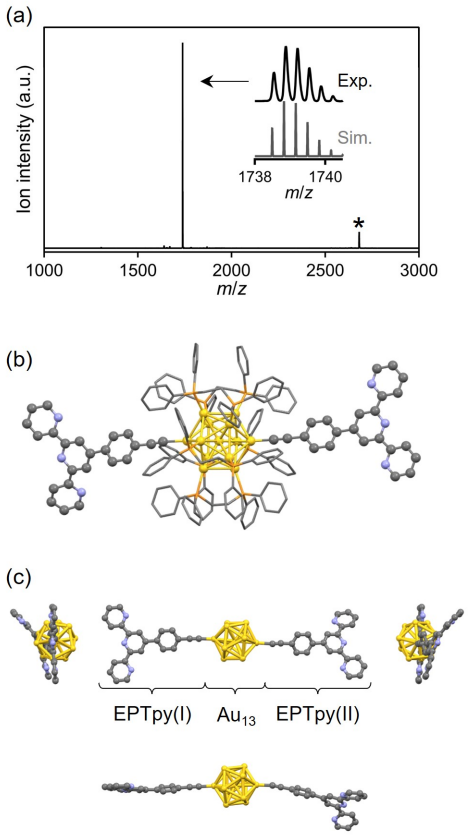

Figure 1. (a) Positive-mode ESI mass spectrum of **2**. The inset compares the experimental peak with the simulated isotope pattern. The peak with an asterisk is assigned as $[\mathbf{2}{\cdot}(PF_6)]^{2+}$. (b) Crystal structure of **2**. Anions and H atoms are omitted, and carbon and phosphorus atoms of dppe moieties are shown as sticks for clarity. Color code: yellow, Au; orange, P; blue, N; gray, C. (c) Multi-directional views of the Au_{13} core and two EPTpy ligands.

The UV-Vis absorption spectrum of **2** differs from that of **1** in the wavelength range of ~400–600 nm (Figure 2b), but is quite similar to that of $[Au_{13}(dppe)_5(PA)_2]^{3+}$.[22] Newly emerged features at around 300 nm (Figure 2a) are assigned to the π–π* transition of the EPTpy moieties, whereas the low-energy transitions at 485 and 525 nm are mainly assigned to the electronic transition from HOMO and HOMO-1 constructed by the superatomic 1P orbitals of the Au_{13} core and the π orbitals of EPTpy, according to the previous theoretical study on $[Au_{13}(dppe)_5(PA)_2]^{3+}$. The PL QY of **2** (0.17) was significantly larger than that of **1** (0.11) as shown in Figure S3, and is comparable to that of $[Au_{13}(dppe)_5(PA)_2]^{3+}$ (0.16).[22]

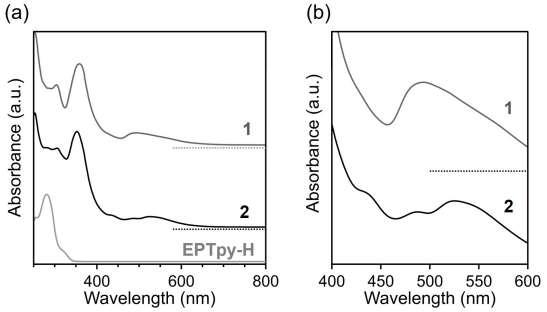

Figure 2. (a) UV-Vis absorption spectra of **1**, **2**, and EPTpy-H. (b) Expanded spectra of **1** and **2** in the range of 400–600 nm.

3.2. Complexation of $[Au_{13}(dppe)_5(EPTpy)_2]^{3+}$ with $M(NO_3)_2$ (M = Co, Ni, Cu, Zn)

The complexation behavior of **2** with Co^{2+} ions in acetonitrile solution was monitored at ambient temperature by ESI-MS. When one molar equivalent of $Co(NO_3)_2{\cdot}6H_2O$ was added to the solution of **2**, new mass peaks assignable to $[\mathbf{2}{\cdot}Co(NO_3)]^{4+}$ (**I**) and $[\mathbf{2}{\cdot}(Co(NO_3))_2]^{5+}$ (**IV**) were observed in addition to that of the unreacted **2** (Figure 3a). These species correspond to the complexation products of one or two $Co(NO_3)^+$ to the terpyridyl moieties of **2**. It is not clear at this moment whether the loss of the NO_3^- ligand from $Co(NO_3)_2$ occurred in the solution or in the ESI source. To gain structural information of the complexation products in solution, the Co K-edge X-ray absorption near edge structure (XANES) spectrum of the acetonitrile solution containing an equimolar amount of **2** and $Co(NO_3)_2{\cdot}6H_2O$ were measured. The XANES spectrum (Figure S4) looked similar to that of $[Co(tpy)_2](PF_6)_2$, but differed significantly from that of $Co(NO_3)_2{\cdot}6H_2O$. This observation indicated that Co^{2+} ions are chelated by the terpyridyl moieties of **2** in solution. More interestingly, dimeric products with the formula of $[\mathbf{2}{\cdot}Co{\cdot}\mathbf{2}]^{8+}$ (**II**), $[\mathbf{2}{\cdot}Co{\cdot}\mathbf{2}{\cdot}Co(NO_3)]^{9+}$ (**III**) and their adducts with PF_6^- were detected in the ESI mass spectra (Figure 3a). Products **II** correspond to a dimer of **2** linked

by the chelation of Co^{2+} ions, while $Co(NO_3)$ is further complexed to one of the terpyridyl moieties of $[\mathbf{2}\cdot Co\cdot\mathbf{2}]^{8+}$ in products **III**. These results indicate that cluster **2** bearing two terpyridyl moieties can be linked together by chelation of the Co^{2+} ions, as we expected. We attempted to observe the 1D linked structure of **2** by TEM. Figure S5 shows a TEM image of a selected area where the particles are well dispersed. Some particles appear to be aligned linearly (Figure 3d). Note that the image of the Au_{13} particles is blurred, suggesting that the atoms within the particles exhibit dynamic rearrangement throughout the 2 s exposure time in TEM imaging.[34] The distances between the adjacent particles were >2.8 nm, which are longer than that expected for the vdW dimer of **2** (~2 nm), but comparable to that estimated for a linked dimer of **2** via Co^{2+} (~3.2 nm). The TEM analysis supports the formation of small multimers of **2** although we could not obtain convincing evidence of the formation of longer linked polymers of **2**. On the other hand, when two molar equivalents of $Co(NO_3)_2\cdot 6H_2O$ were added to the solution of **2**, product **IV** and the complexes with one or two NO_3^- dominated the positive-mode ESI mass spectra: the mass peak of $\mathbf{2}^{3+}$ completely disappeared (Figure 3b). The absence of mass peaks containing more than two Co^{2+} ions is consistent with our assumption that two terpyridyl moieties on cluster **2** provide coordination sites for the Co^{2+} ions.

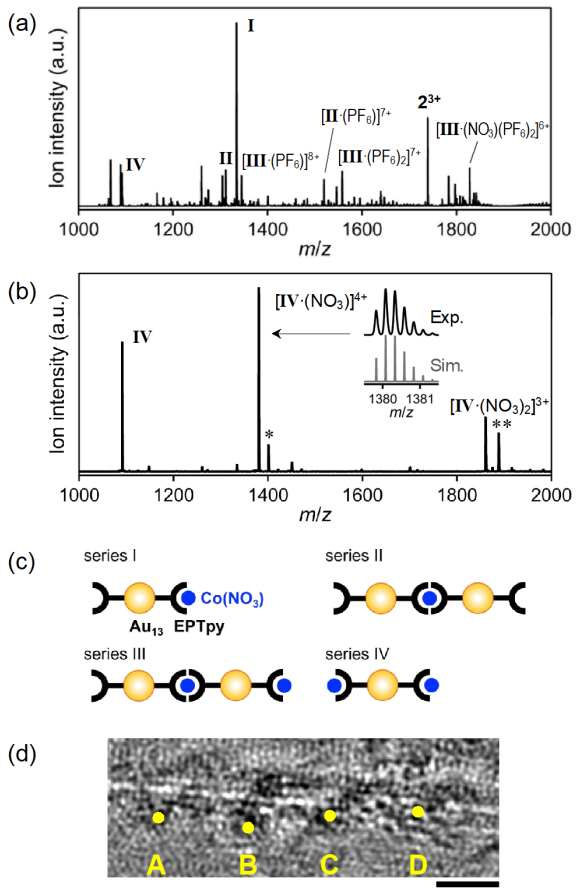

Figure 3. Positive-mode ESI mass spectrum of **2** after the addition of (a) one and (b) two molar equivalents of $Co(NO_3)_2\cdot 6H_2O$. The peaks marked with * and ** in panel (b) are assigned to $[\mathbf{IV}\cdot(PF_6)]^{4+}$ and $[\mathbf{IV}\cdot(NO_3)(PF_6)]^{3+}$, respectively. (c) Schematic representation of the four series of products is given on the right: $[\mathbf{2}\cdot Co(NO_3)]^{4+}$ (**I**); $[\mathbf{2}\cdot Co\cdot\mathbf{2}]^{8+}$ (**II**); $[\mathbf{2}\cdot Co\cdot\mathbf{2}\cdot Co(NO_3)]^{9+}$ (**III**); $[\mathbf{2}\cdot(Co(NO_3))_2]^{5+}$ (**IV**). (d) TEM image of the mixture of equal molar amounts of **2** and $Co(NO_3)_2\cdot 6H_2O$. The yellow dots represent the center of four particles A–D. The measured A–B, B–C, and C–D distances are 3.11, 2.93, and 3.15 nm, respectively. Scale bar: 2 nm.

Cluster **2** showed a similar complexation behavior with other 3d metal ions such as Ni^{2+}, Cu^{2+}, and Zn^{2+}. When two molar equivalents of $M(NO_3)_2\cdot nH_2O$ (n = 6 for M = Ni^{2+} and Zn^{2+}; n = 3 for M = Cu^{2+}) were added to the solution of **2**, we observed the complexation of two metal ions to individual **2** in the ESI mass spectra (Figure S6). These results indicate that the terpyridyl moieties of **2** can capture two 3d metal ions (Co^{2+}, Ni^{2+}, Cu^{2+}, and Zn^{2+}) equivalently.

3.3. Modulation of optical properties of $[Au_{13}(dppe)_5(EPTpy)_2]^{3+}$ by coordination of metal ions

The addition of M^{2+} (M = Co, Ni, Cu, Zn) ions affected the optical properties of **2**. The UV-Vis absorption spectra of **2** changed slightly but clearly upon the successive addition of $Co(NO_3)_2\cdot 6H_2O$ (Figure 4a). The complexation with Co^{2+} ions suppressed the ligand-centered absorption by EPTpy moieties at ~280–350 nm and enhanced the absorbance at ~350–600 nm, probably due to the LMCT transition of the Co^{2+}–terpyridyl moieties. The absorbance at 358 nm successively increased during zero to two molar equivalents and reached a plateau after two molar equivalents (Figure 4c). This suggests that the spectral shift was caused by the complexation reaction and saturated after two EPTpy moieties were bonded to the Co^{2+} ions. A similar change in the optical spectral profiles was observed upon coordination of Ni^{2+}, Cu^{2+}, and Zn^{2+} (Figure S7).

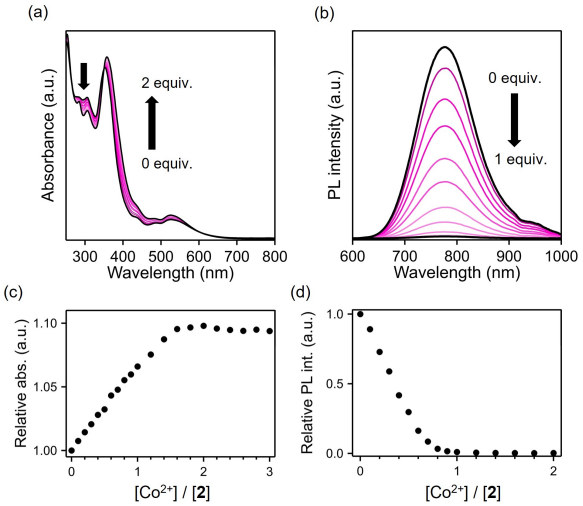

Figure 4. (a) UV-Vis absorption spectra of **2** with zero to two molar equivalents of Co^{2+}. (b) PL spectra (λ_{ex} = 525 nm, normalized by the absorption at 525 nm) of **2** with zero to one molar equivalents of Co^{2+}. (c) Plot of the absorbance at 358 nm relative to the original solution of **2**. (d) Plot of the PL intensity at 780 nm relative to the original solution of **2**.

In contrast, the impact on the PL properties of **2** depended remarkably on the coordinated metal ions. The successive addition of $Co(NO_3)_2\cdot 6H_2O$ suppressed the PL from the Au_{13} core while maintaining the peak position at ~780 nm (Figure 4b). The PL intensity at 780 nm monotonically decreased by adding Co^{2+} and became negligible after adding about one molar equivalent of Co^{2+} (Figure 4d). This suggests that the PL from the Au_{13} core is suppressed by the complexation with Co^{2+} and is almost completely quenched when at least one of the EPTpy ligands is bound to Co^{2+} (Figures 4d, 5a). This result indicates that complexation with the Co^{2+} ions quenches the PL from the Au_{13} core. The PL intensity of **2** at ~780 nm also decreased to <1% of the original solution after adding two molar equivalents of Ni^{2+} and Cu^{2+} (Figures 5b, c). On the other hand, the

complexation of Zn^{2+} did not affect the PL intensity (Figure 5d).

The PL quenching might have proceeded in a non-destructive manner. As the addition of Co^{2+} and Zn^{2+} did not cause a significant decomposition of Au_{13} (Figure S8), the PL lifetime of **2** before and after complexation with Co^{2+} and Zn^{2+} was analyzed by fitting the PL decay profiles with a single exponential function (Figure S9, Table 1). The PL lifetime of **2** was calculated to be 3.66 μs, slightly longer than that of **1** (2.78 μs). The PL lifetime of **2** was significantly shortened to 19.6 ns upon complexation with two molar equivalents of Co^{2+}, while it remained comparable (3.41 μs) upon complexation with two molar equivalents of Zn^{2+}. This indicates that the nonradiative decay of the photoexcited Au_{13} core is enhanced by a specific complexation with Co^{2+}.

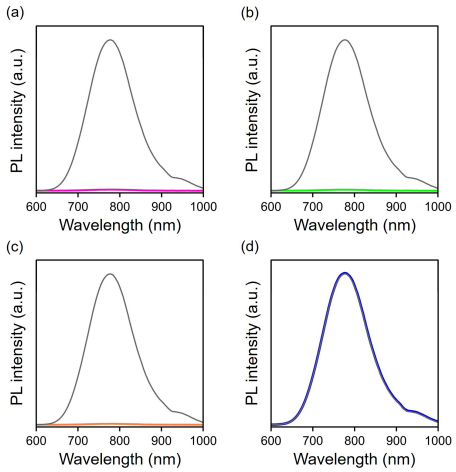

Figure 5. PL spectra (λ_{ex} = 525 nm) of **2** before (gray) and after (colored) adding two molar equivalents of (a) Co^{2+}, (b) Ni^{2+}, (c) Cu^{2+}, and (d) Zn^{2+}.

Table 1. PL lifetime

	1	**2**	**2** + Co^{2+}	**2** + Zn^{2+}
τ^a (μs)	2.78	3.66	0.02	3.41

a: τ was calculated by fitting the decay profile with single exponential functions.

The metal-dependent PL quenching phenomenon is explained by the difference in the electronic structures of metal ions:[35,36] the electron configurations of Co^{2+}, Ni^{2+}, Cu^{2+}, and Zn^{2+} are d^7, d^8, d^9, and d^{10}, respectively. Figure 6a schematically shows a proposed mechanism of PL quenching by complexation with Co^{2+}. Previous studies on the PL properties of **1** suggested that the photoexcited state of **2** is quickly converted to a triplet state via rapid intersystem crossing. Then, the exciton energy of the Au_{13} core is transferred to metal d-d centered excited states of Co^{2+}, which decays nonradiatively. It is worth noting that oxygen molecules in the air are not involved in the PL quenching mechanism (Figure S10). We speculate that this energy transfer from the Au_{13} core to the chelated Co^{2+} proceeds via electron exchange between them (Figure 6b): the electron in the lowest unoccupied molecular orbital (LUMO) of the Au_{13} moiety is transferred to the unoccupied 3d orbital of Co^{2+}, while the electron in the 3d orbital of Co^{2+} is transferred to the HOMO of the Au_{13} moiety. However, this electron exchange is impossible between the Au_{13} moiety and Zn^{2+} because of the closed electron configuration (d^{10}) of Zn^{2+} (Figure 6b). Quantum chemical calculations are needed to prove the electronic conjugation between Au_{13} and Co^{2+} ions via alkynyl groups. Unfortunately, this theoretical calculation is beyond the scope of this paper because computational resources for studying such a large system are limited and insufficient information on the coordination environment of the Co^{2+} ion is available to construct a reasonable model structure.

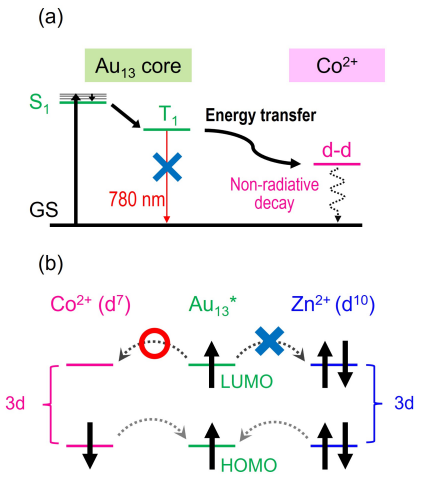

Figure 6. (a) Proposed mechanism of PL quenching of **2** coordinating with Co^{2+}. (b) Schematic illustration of the electronic interaction between the excited Au_{13} core and M^{2+} (M = Co, Zn).

4. Conclusion

We successfully introduced two terpyridine-functionalized alkynyl ligands (EPTpy) at the diagonal apex sites of an icosahedral Au_{13} superatom protected by diphosphine (dppe) ligands. The electronic coupling between the π systems of the EPTpy ligands and the superatomic orbitals of Au_{13} resulted in a spectral shift and the enhancement of the visible (~780 nm) photoluminescence quantum yield from 11 to 17%. The addition of one molar equivalent of Co^{2+} to $[Au_{13}(dppe)_5(EPTpy)_2]^{3+}$ (**2**) induced the dimerization of **2** via chelation of Co^{2+} at the terpyridyl moieties. The addition of two molar equivalents of Co^{2+} selectively yielded the complexes $[\mathbf{2}{\cdot}Co_2(NO_3)_x]^{(7-x)+}$. The complexation caused modulation of the absorption spectra and nearly complete quenching of the PL. This phenomenon is explained in terms of energy transfer from the Au_{13} chromophore to the coordinated Co^{2+} ions. Complete PL quenching was also observed by the complexation of Ni^{2+} and Cu^{2+}, while the complexation of Zn^{2+} did not affect the PL intensity. This exceptional behavior of Zn^{2+} can be rationalized by the closure of the 3d orbitals. These findings suggest that cluster **2** can be used for sensing of specific metal ions. Cluster **2** is a potential candidate for the building units for a higher order of superatomic systems with novel functionalities.

Acknowledgment

We thank Prof. Tomohiro Shiraki (Kyushu University) for providing us with purified BNNT, and Dr. Koji Kimoto (NIMS) for his assistance with the 40 kV TEM observation. This research was supported financially by JST, CREST (GrantJPMJCR20B2) and by JSPS KAKENHI Grants JP20H00370, JP23H01917 and JP23H04874. The SCXRD experiment was supported by the Nanotechnology Platform Program (Advanced Characterization Nanotechnology Platform, Project JPMXP09A20UT0024) of the Ministry of Education, Culture, Sports, Science and Technology (MEXT), Japan. The synchrotron radiation experiments were performed with the approval (Approval No. 2021A1200) of the Japan Synchrotron Radiation Research Institute (JASRI).

References

1. R. Jin, C. Zeng, M. Zhou, Y. Chen, *Chem. Rev.* **2016**, *116*, 10346.
2. I. Chakraborty, T. Pradeep, *Chem. Rev.* **2017**, *117*, 8208.
3. T. Omoda, S. Takano, T. Tsukuda, *Small* **2021**, *17*, 2170136.
4. S. Takano, T. Tsukuda, *J. Am. Chem. Soc.* **2021**, *143*, 1683.
5. X. Kang, Y. Li, M. Zhu, R. Jin, *Chem. Soc. Rev.* **2020**, *49*, 6443.
6. B. Zhang, J. Chen, Y. Cao, O. J. H. Chai, J. Xie, *Small* **2021**, *17*, 2004381.
7. X. Kang, M. Zhu, *Chem. Soc. Rev.* **2019**, *48*, 2422.
8. X. Kang, M. Zhu, *Coord. Chem. Rev.* **2019**, *394*, 1.
9. Z. Wu, Q. Yao, S. Zang, J. Xie, *ACS Mater. Lett.* **2019**, *1*, 237.
10. A. Ebina, S. Hossain, H. Horihata, S. Ozaki, S. Kato, T. Kawawaki, Y. Negishi, *Nanomater.* **2020**, *10*, 1105.
11. Y. Saito, C. Murata, M. Sugiuchi, Y. Shichibu, K. Konishi, *Coord. Chem. Rev.* **2022**, *470*, 214713.
12. Nonappa, T. Lahtinen, Johannes. S. Haataja, T. Tero, H. Häkkinen, O. Ikkala, *Angew. Chem. Int. Ed.* **2016**, *55*, 16035.
13. M. D. Nardi, S. Antonello, D. Jiang, F. Pan, K. Rissanen, M. Ruzzi, A. Venzo, A. Zoleo, F. Maran, *ACS Nano* **2014**, *8*, 8505.
14. Z. Wu, Y. Du, J. Liu, Q. Yao, T. Chen, Y. Cao, H. Zhang, J. Xie, *Angew. Chem. Int. Ed.* **2019**, *58*, 8139.
15. T. Lahtinen, E. Hulkko, K. Sokołowska, T.-R. Tero, V. Saarnio, J. Lindgren, M. Pettersson, H. Häkkinen, L. Lehtovaara, *Nanoscale* **2016**, *8*, 18665.
16. A. Sels, G. Salassa, F. Cousin, L.-T. Lee, T. Bürgi, *Nanoscale* **2018**, *10*, 12754.
17. G. Chelucci, R. P. Thummel, *Chem. Rev.* **2002**, *102*, 3129.
18. E. C. Constable, *Chem. Soc. Rev.* **2007**, *36*, 246.
19. U. S. Schubert, C. Eschbaumer, *Angew. Chem. Int. Ed.* **2002**, *41*, 2892.
20. H. Hofmeier, U. S. Schubert, *Chem. Soc. Rev.* **2004**, *33*, 373.
21. S. Chakraborty, G. R. Newkome, *Chem. Soc. Rev.* **2018**, *47*, 3991.
22. M. Sugiuchi, Y. Shichibu, T. Nakanishi, Y. Hasegawa, K. Konishi, *Chem. Commun.* **2015**, *51*, 13519.
23. Y. Shichibu, K. Konishi, *Small* **2010**, *6*, 1216.
24. M. Mitsui, D. Arima, A. Uchida, K. Yoshida, Y. Arai, K. Kawasaki, Y. Niihori, *J. Phys. Chem. Lett.* **2022**, *13*, 9272.
25. A. Leyva-Pérez, A. Doménech-Carbó, A. Corma, *Nat. Commun.* **2015**, *6*, 6703.
26. D. Qiu, M. Li, Q. Zhao, H. Wang, C. Yang, *Inorg. Chem.* **2015**, *54*, 7774.
27. E. C. Constable, K. Harris, C. E. Housecroft, M. Neuburger, J. A. Zampese, *CrystEngComm.* **2010**, *12*, 2949.
28. M. Strohalm, D. Kavan, P. Novák, M. Volný, V. Havlíček, *Anal. Chem.* **2010**, *82*, 4648.
29. G. M. Sheldrick, *Acta Cryst. C* **2015**, *71*, 3.
30. P. van der Sluis, A. L. Spek, *Acta Cryst. A* **1990**, *46*, 194.
31. A. L. Spek, *J. Appl. Cryst.* **2003**, *36*, 7.
32. T. Shiraki, R. Saito, H. Saeki, N. Tanaka, K. Harano, T. Fujigaya, *Chem. Lett.* **2023**, *52*, 44.
33. O. J. G. L. Chevalier, T. Nakamuro, W. Sato, S. Miyashita, T. Chiba, J. Kido, R. Shang, E. Nakamura, *J. Am. Chem. Soc.* **2022**, *144*, 21146.
34. Hasegawa, S. Masuda, S. Takano, K. Harano, J. Kikkawa, T. Tsukuda, *ACS Nano* **2022**, *16*, 16932.
35. L. Fabbrizzi, M. Licchelli, P. Pallavicini, A. Perotti, A. Taglietti, D. Sacchi, *Chem. Eur. J.* **1996**, *2*, 75.
36. R. Bergonzi, L. Fabbrizzi, M. Licchelli, C. Mangano, *Coord. Chem. Rev.* **1998**, *170*, 31.